42nd AIAA Fluid Dynamics Conference and Exhibit
25 - 28 June 2012, New Orleans, Louisiana

AIAA 2012-3252

A numerical method for DNS of turbulent reacting flows using complex chemistry

Rajapandiyan Asaithambi* , Suman Muppidi † and Krishnan Mahesh‡

Aerospace Engineering and Mechanics, University of Minnesota,

Minneapolis, MN 55455-0513, USA

A novel compressible Navier-Stokes solver for chemically reacting flows is proposed with an explicit Navier-Stokes predictor step and a semi-implicit corrector step for stiff chemical source terms. A modular code to read chemical mechanisms in the Chemkin format is coupled to the solver allowing the ability to simulate multiple fuels with minimal effort. This segregated approach allows the independent modification of the Navier-Stokes solver and the chemical source term integration algorithm. Validation of a well-stirred reactor, an unsteady unstrained diffusion flame, and results from a lifted non-premixed flame in vitiated coflow in two and three dimensional configurations are presented.

I. Introduction

Combustion is central to many applications, including automotive and gas turbine engines, and various burners. These applications involve turbulent transport of various species which directly affects the chemical process and it is imperative that accurate numerical simulations reliably capture this interaction. The design of the next generation of engines aimed at efficient combustion and reduced pollutants such as NO_x can benefit from these high-fidelity computations. Simulations of combustion using Reynolds Averaged Navier Stokes (RANS) equations are computationally efficient but may not be accurate enough for turbulent reacting flows.[1] Large Eddy Simulations (LES) and Direct Numerical Simulations (DNS) are very accurate but require suitable numerical techniques while also being computationally expensive. We are developing the capability to perform DNS/LES of turbulent reacting flows in complex geometries.

The challenge in simulating turbulent reacting flows arises from the stiffness imposed by chemical time scales in addition to the turbulent length scales and extra species equations. In Doom, Hou and Mahesh[2] the species source term was linearized and made semi-implicit which allowed the stiffness from chemistry to be vastly reduced, allowing the reduction of the time step Δt by a factor of 10^5 for hydrogen chemistry. The algorithm was then applied to autoignition of hydrogen vortex rings in Doom & Mahesh.[3] The solver is an implicit projection-based method for all Mach numbers. An unstructured explicit solver derived from Park & Mahesh[4] has been used in very large complex geometries, includes a robust modified least squares flux reconstruction, a shock-capturing scheme and subgrid-scale modelling. We propose a hybrid density based approach where we retain the explicit method of Park & Mahesh[4] for advection and diffusion and integrate the chemical source term using the semi-implicit method of Doom, Hou & Mahesh.[2] The species equation is solved in two steps with advection-diffusion being the explicitly advanced predictor step. The linearized chemical source terms are solved implicitly in the corrector step by iterating till convergence is obtained. The implicit step does not affect any spatial operator and therefore does not suffer from the computational overhead that fully implicit methods do. This algorithm is suited for high speed subsonic reacting flows where the viscous wall limitations are not encountered such as jets. In addition, a new chemistry module is designed to read in detailed Chemkin input files and automatically linearize source terms. This allows us to plug in arbitrary reaction mechanisms to the code and obtain results for various fuel/oxidizer combinations. With access to tabulated thermodynamic properties, chemical species can have realistic heat capacities as a function of temperature.

*Graduate Research Assistant, Aerospace Engineering and Mechanics, University of Minnesota, AIAA Student Member
†Research Associate, Aerospace Engineering and Mechanics, University of Minnesota, AIAA Member
‡Professor, Aerospace Engineering and Mechanics, University of Minnesota, AIAA Associate Fellow

To demonstrate the algorithm we simulate a category of flames that has been the focus of extensive experimental and numerical study. The experimental flames designed by Cabra et al.,[5] Dally et al.,[6] Mastorakos et al.[7] and Oldenhof et al.[8] autoignite, where no external heat source is necessary to initiate combustion. These experiments were inspired by compression engines, where there is a need to understand the ignition of fuel jets when injected into a hot oxidizer. These flames pose a challenge to current modelling techniques[9] and DNS of such flames could help better understand the turbulence-chemistry interaction and aid the development and validation of models.

II. Numerical Details

II.A. Governing Equations

The governing equations for an ideal thermally perfect gas are written down below. The energy equation is written for the total chemical energy and therefore the equation does not have an explicit chemical heat release term.

$$\frac{\partial \rho^d}{\partial t^d} + \frac{\partial \rho u_j^d}{\partial x_j^d} = 0 \tag{1}$$

$$\frac{\partial \rho^d Y_k}{\partial t^d} + \frac{\partial \rho^d Y_k u_j^d}{\partial x_j^d} = \frac{\partial}{\partial x_j^d}\left(\rho^d D_k^d \frac{\partial Y_k}{\partial x_j^d}\right) + \dot{\omega}_k^d \tag{2}$$

$$\frac{\partial g_i^d}{\partial t^d} + \frac{\partial g_i^d u_j^d}{\partial x_j^d} = -\frac{\partial p^d}{\partial x_j^d} + \frac{\partial \tau_{ij}^d}{\partial x_j^d} \tag{3}$$

$$\frac{\partial \rho^d E_t^d}{\partial t^d} + \frac{\partial}{\partial x_j^d}\left(\rho^d E_t^d + p^d\right) u_j^d = \frac{\partial \tau_{ij}^d u_i^d}{\partial x_j^d} + \frac{\partial}{\partial x_j^d}\left(k^d \frac{\partial T^d}{\partial x_j^d}\right) \tag{4}$$

where

$$\tau_{ij}^d = \mu^d \left(\frac{\partial u_i^d}{\partial x_j^d} + \frac{\partial u_j^d}{\partial x_i^d} - \frac{2}{3}\frac{\partial u_k^d}{\partial x_k^d}\delta_{ij}\right) \tag{5}$$

$$E_t^d = e_t^d + \frac{u_i^d u_i^d}{2} = h_t^d - p^d/\rho^d + \frac{u_i^d u_i^d}{2} \tag{6}$$

$$h_t^d = \int_{T_o^d}^{T^d} c_p^d(Y_k, T'^d) dT'^d + \sum_{k=1}^{n} \triangle h_{f,k}^o{}^d Y_k \tag{7}$$

The superscript 'd' is used to denote dimensional quantities. We can non-dimensionalize these equations with reference quantities denoted with the subscript 'r' as follows:

$$t = \frac{t^d}{L_r/u_r}, x = \frac{x^d}{L_r}, \rho = \frac{\rho^d}{\rho_r}, u_i = \frac{u_i^d}{u_r}, g_i = \frac{g_i^d}{\rho_r u_r}, \mu = \frac{\mu^d}{\mu_r}, p = \frac{p^d}{\rho_r u_r^2}, T = \frac{T^d}{T_r}, \dot{\omega}_k = \frac{L_r}{\rho_r u_r}\dot{\omega}_k^d \tag{8}$$

$$R = \frac{R^d}{R_r}, W = \frac{W^d}{W_r}, c_p = \frac{c_p^d}{R_r}, h = \frac{h^d}{R_r T_r}, M_r = \frac{u_r}{c_r}, p_r = \rho_r R_r T_r, R_r = \frac{R_{univ}}{W_r}, c_r^2 = \gamma_r R_r T_r \tag{9}$$

$$Re = \frac{\rho_r u_r L_r}{\mu_r}, Sc_k = \frac{\mu^d}{\rho^d D_k^d}, Pr = \frac{\mu^d c_p^d}{k^d} \tag{10}$$

The reference quantities that need to be chosen are a length scale L_r, a velocity scale by choosing M_r and the thermodynamic properties: pressure p_r, temperature T_r, and viscosity (by choosing Re) based on a reference mixture Y_{k_r}.

The non-dimensional form of the equations are now written down:

$$\frac{\partial \rho}{\partial t} + \frac{\partial \rho u_j}{\partial x_j} = 0 \tag{11}$$

$$\frac{\partial \rho Y_k}{\partial t} + \frac{\partial \rho Y_k u_j}{\partial x_j} = \frac{1}{ReSc_k}\frac{\partial}{\partial x_j}\left(\mu \frac{\partial Y_k}{\partial x_j}\right) + \dot{\omega}_k \tag{12}$$

$$\frac{\partial g_i}{\partial t} + \frac{\partial g_i u_j}{\partial x_j} = -\frac{\partial p}{\partial x_j} + \frac{1}{Re}\frac{\partial \tau_{ij}}{\partial x_j} \tag{13}$$

$$\frac{\partial \rho E_t}{\partial t} + \frac{\partial}{\partial x_j}\left(\rho E_t + p\right) u_j = \frac{1}{Re}\frac{\partial \tau_{ij} u_i}{\partial x_j} + \frac{1}{\gamma_r M_r^2 RePr}\frac{\partial}{\partial x_j}\left(\mu c_p \frac{\partial T}{\partial x_j}\right) \tag{14}$$

The non-dimensional equation of state is:

$$\rho T = \gamma_r M_r^2 p W \tag{15}$$

II.B. Numerical Method

The algorithm is a second order scheme in space and time, and colocated allowing the method to be applied for a structured or unstructured finite volume grid. Symmetric average flux reconstruction, as described by Park & Mahesh,[4] of cell centered variables is used to obtain the values at faces in the structured solver whereas the unstructured solver uses the modified least-square method. Time advancement of the equations is dealt with a two step predictor-corrector method. The advection and diffusion terms are advanced using a second-order explicit Adams-Bashforth scheme. The stiff chemical source terms employ a second-order semi-implicit discretization as described in Doom & Mahesh.[2]

The following equations are explicitly solved in the predictor step:

$$\frac{\partial \rho}{\partial t} = -\frac{1}{V_f}\sum_{faces} \rho_f v_n A_f \tag{16}$$

$$\frac{\partial \rho Y_k}{\partial t} = -\frac{1}{V_f}\sum_{faces} \left[\rho_f Y_{k,f} v_n + J_{k,f} n_k\right] A_f \tag{17}$$

$$\frac{\partial g_i}{\partial t} = -\frac{1}{V_f}\sum_{faces} \left[g_{i,f} v_n + p_f n_i - \frac{1}{Re}\tau_{ik,f} n_k\right] A_f \tag{18}$$

$$\frac{\partial \rho E_t}{\partial t} = -\frac{1}{V_f}\sum_{faces} \left[\left(\rho E_t + p\right) v_n - \frac{1}{Re}\tau_{ik,f} u_{i,f} n_k - Q_{k,f} n_k\right] A_f \tag{19}$$

These equations are solved with the following Adams-Bashforth time discretization and we get the density ρ, mass fractions $\hat{Y}_k$, momentum g_i and total chemical energy ρE_t for all the cells at time $(t+1)$.

$$q^{n+1} = q^n + \frac{\Delta t}{2}\left[3 * rhs^n(q) - rhs^{n-1}(q)\right] \tag{20}$$

Note that the species equation is solved without the source term $\dot{\omega}_k$ and thus the explicit step gives us $\rho\hat{Y}_k$. This predicted species density has to be corrected to include the effect of chemical reactions from the source term $\dot{\omega}_k$. The stiff chemical source terms are linearized to make this term implicit which is then iteratively solved. The source term only affects the species equations; the mass, momentum and energy are not affected and this allows us to decouple the source term in a special way. Since the quantities ρ^{t+1}, g_i^{t+1} and E_t^{t+1} are already known, we can obtain the chemical energy e_t^{t+1}. The change in species concentrations due to the chemical source terms therefore is an ordinary differential equation with the constraint e_t^{t+1} that the new mass fractions Y_k^{t+1} and T^{t+1} have to obey. The correction for source terms is written:

$$\frac{(\rho Y_k)^{t+1,p} - (\rho\hat{Y}_k)^{t+1})}{\Delta t} = \dot{\omega}_k((\rho Y_k)^t, (\rho Y_k)^{t+1,p}, (T)^t, (T)^{t+1,p}) = (\dot{\omega}_k)_L (\rho Y_k)^{t+1,p} + (\dot{\omega}_k)_R \tag{21}$$

The linearization of $\dot{\omega}_k$ is done in a separate code module which parses Chemkin mechanism and thermodynamic data files and computes linearized source terms. The two equations we need to iteratively solve in the corrector step are:

$$(\rho Y_k)^{t+1,p} = \frac{(\rho \hat{Y_k})^{t+1} + \Delta t(\dot{\omega}_k)_R}{1 + \Delta t(\dot{\omega}_k)_L} \tag{22}$$

$$T^{t+1,p} = f^{-1}({e_t}^{t+1}, {Y_k}^{t+1,p}) \tag{23}$$

This step yields the final species mass fractions and temperature at the new time step $(t+1)$. The enthalpy necessary to calculate e_t is obtained directly from thermodynamic property tables as a function of temperature and species concentrations. Since e_t and h_t are both purely functions of temperature and species composition and we are trying to estimate the temperature from equation 23, this step involves a mutlivariate root finding method. Halley's method is used for its faster convergence as compared to Newton-Raphson.

III. Results

The algorithm is applied to four closely related problems with a logical progression in complexity. The first is a well-stirred reactor, without any spatial variations: a zero-dimensional problem with evolution in time only. The equations reduce to a set of ordinary differential equations and this serves as a validation for the chemical source terms. The results are compared with Chemkin for two different fuels. The second problem is an unsteady unstrained one-dimensional diffusion flame which couples chemistry with spatial variation. The last two problems are a two-dimensional jet flame and a three-dimensional round jet flame. The two-dimensional jet serves as a useful tool to understand and evaluate the behavior of various fuels and is computationally cost-effective. The three-dimensional round jet can however directly address experimental studies.

Note: All problems in this paper implicitly take the fuel inlet conditions to be the reference mixture at Mach number, $M_r = 1$, temperature $T_r = 298K$ and pressure $p_r = 1atm$. The reference length scale is $L_r = 0.005m$ which is representative of the problems that will be presented below. The jet diameter (for 2D and 3D) is thus taken to be $5mm$. All quantities are non-dimensional unless units are explicitly noted.

III.A. Well Stirred Reactor

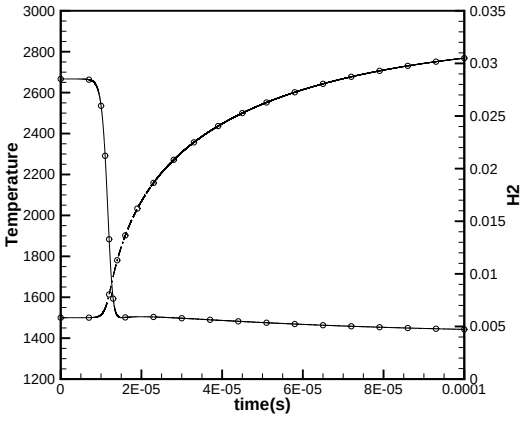

Figure 1. $H_2 - Air$ **Mueller Mechanism.**

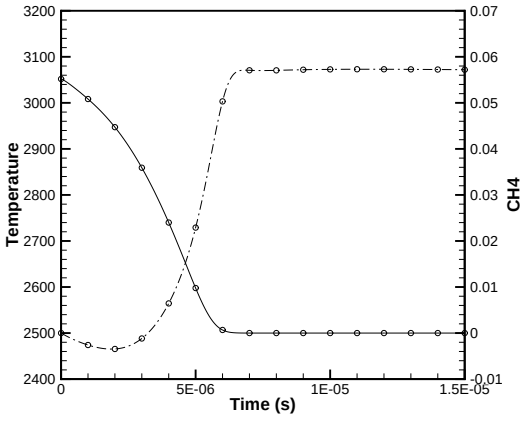

Figure 2. $CH_4 - Air$ **GRI-Mech.**

The well-stirred reactor (0D combustion) is a temporally accurate solution to a set of initial conditions and the mixture reaches an equilibrium temperature. A hydrogen-air mixture at $1500K$ and a methane-air mixture at $2500K$, both at stoichoimetric ratios and atmospheric pressure, are simulated. In figures 1 and 2, the results obtained (straight lines) are compared with Chemkin (dots) where we are able to get

excellent agreement. The simulations use detailed reaction mechanisms for both fuels: hydrogen, which uses a 9 species, 19 reaction Mueller et. al. mechanism[10] and methane, which uses the full GRI-Mech 3.0[11] mechanism with 53 species and 325 reactions. This demonstrates the black-box ability of the chemistry module to solve a wide range of chemical mechanisms. In the jet flames described further below we use this flexibility to study three different fuels in the same configuration.

III.B. One-dimensional unsteady unstrained diffusion flame

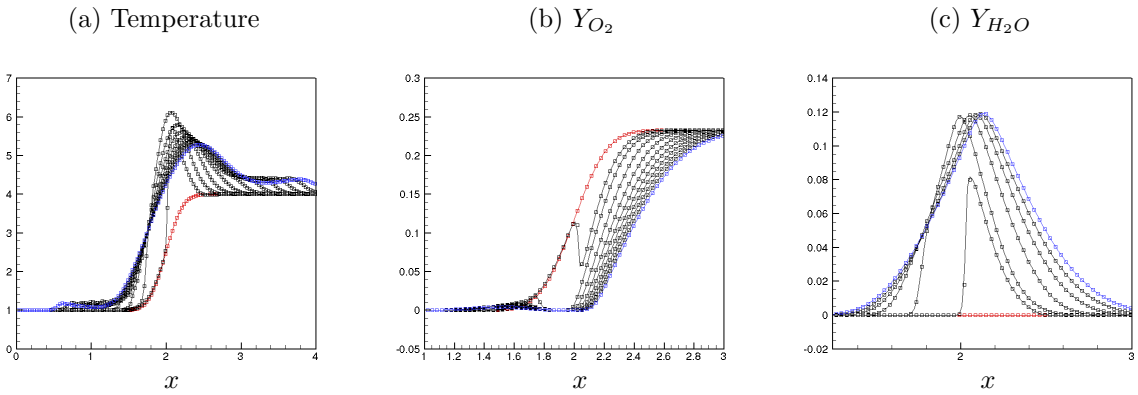

Figure 3. Comparison of $1D$ unstrained diffusion flame results from the structured (□) and unstructed (–) solvers.

An unsteady unstrained one-dimensional diffusion flame with cold fuel (H_2/N_2 at $T = 1$) and hot oxidizer (Air at $T = 4$) on either ends allows autoignition of fuel at the interface. No 'numerical spark' is needed to start the combustion, which quickly stabilizes into a diffusion flame and slowly evolves. The initial temperature and mixture fraction curve is a profile given by:

$$T(x) = \frac{T_f - T_o}{2}\left[1 - \tanh\left(\frac{x-2}{0.1}\right)\right] + T_o \tag{24}$$

$$\zeta(x) = \frac{\zeta_f - \zeta_o}{2}\left[1 - \tanh\left(\frac{x-2}{0.1}\right)\right] + \zeta_o \tag{25}$$

Fuel	T_{fuel}	T_{air}	Y_{fuel}	Y_{O_2}	Re
H_2	1	4	0.029	0.233	1000

Table 1. Initial conditions for the unsteady one-dimensional flame.

In figure 3, the red lines are the initial profiles and blue lines are the profiles at $0.1s$. The initial mass fractions are 0.029 for hydrogen on the cold fuel end (left half) and 0.233 for oxygen of the hot oxidizer end (right half) and the rest filled up with nitrogen (Table 1). The mass fraction of H_2O peaks at 0.12 for the diffusion flame at $t = 0.1s$. After the autoignition phase, the production of H_2O is limited by diffusion of fuel and oxidizer into the flame, thus slowly losing heat while expanding in thickness.

III.C. Two-dimensional unsteady reacting jet

Extending the idea of an autoigniting flame to two dimensions leads to a jet in place of a diffusion flame. Cold nitrogen diluted fuel is injected into hot ambient air and this problem has practical applications from compression ignition engines to various combustors with hot product recirculation. The 'vitiated coflow burner'[5] and the 'jet in hot coflow'[6] burner are model flames to study such applications.

A cold fuel jet at $M_{jet} = 0.3$ issues into heated air with a coflow at $M_{co} = 0.1$. Three fuels: hydrogen, methane, and ethylene are simulated in a 2D slot-jet like geometry. The hydrogen jet uses the 9 species Mueller et. al. mechanism,[10] a 17-species skeletal mechanism[12] for methane and a 22-species reduced mechanism[13] for ethylene are chosen. Table 2 below lists the inlet conditions for the jet and the coflow. The

jet and coflow velocities are same across the different fuels. The inlet velocity profile is given by the following equation with thickness $\delta = 0.01H$:

$$u_{in} = \frac{u_{jet} - u_{coflow}}{2}\left[1 - \tanh\left(\frac{|y| - H/2}{2\delta}\right)\right] + u_{coflow} \tag{26}$$

Non-reflecting far field boundary conditions[14] are applied at the other three boundaries. The domain is $40D\times$ $40D$ in the stream-wise and span-wise direction. Figure 4 is a temperature contour plot of the three jets with a part of the domain is shown. The fuels show different behavior with hydrogen sustaining a stable lifted flame whereas the hydrocarbons only exhibit small kernels of autoignition. The hotter coflow needed to ignite the hydrocarbons has the effect of reducing the coflow density, which leads to thicker shear layers with reduced reaction rates. This effect was the reason to increase the Reynolds number of the hydrocarbon jets to 7200 from the original 3600 which increased roll-up and mixing along the shear layer.

Fuel	T_{fuel}	T_{air}	Y_{fuel}	Y_{O_2}	Re	U_{jet}	U_c
H_2	1	3.5	0.029	0.233	3600	0.3	0.1
CH_4	1	5.0	0.055	0.220	7200	0.3	0.1
C_2H_4	1	5.5	0.082	0.299	7200	0.3	0.1

Table 2. Fuels and their respective inlet conditions.

In figure 5, an autoigniting kernel in each fuel jet is shown. The temperature contours (labelled T) identify the flame with a temperature much hotter than both the fuel and oxidizer streams. Y_{OH}, a species that can be measured in experiments, is a much better indicator of the flame location. Similar correlation with the flame is also observed for the major combustion products Y_{H_2O}, Y_{CO_2}. Y_{CO} is shown for the ethylene flame as it also a species measured in experiments and plays a role in hydrocarbon oxidation. The fuel contours show a local depletion at the flame location. Y_{HO_2} for the hydrogen kernel has high concentrations surrounding the kernel but not inside it, this species breaks down in high temperature zones but plays an important role by aiding formation of intermediates at lower temperatures.

For the hydrogen-air jet, a scatter plot of temperature against the mixture fraction (at every computational volume) over different regions of the computational domain is shown in figure 6. Towards the left half of the domain, $x < 20H$, figure 6(a) shows the absence of any chemical reaction. Figure 6(b) roughly corresponds to the location of contours shown in figure 5 (a) depicting the autoignition of fuel; note that autoignition appears to begin at lean, relatively hotter regions of the flow, the most reactive mixture fraction ζ_{mr},[15] and the reaction then spreads to the fuel-rich regions (as observed in figure 6(c)). Figure 6(d), corresponding to the right half of the domain, indicates that the lean mixture is completely burnt (noted by high temperature) and that the domain contains a significant amount of unburnt, fuel-rich region.

An interesting aspect of this lifted flame is the flame base dynamics at the center of the domain. Here, the flame front appears to leapfrog a vortex pair upstream of it, and while it grows hotter it also gets advected downstream before it makes the jump again over the next pair of vortices. Figure 7 illustrates this process with a sequence of frames from $\tau_j = 180$ to $\tau_j = 195$, where τ_j is the non-dimensional time taken for the jet to cover one jet diameter. The corresponding Y_{HO_2} contours reveals more about this peculiar leapfrogging. There is a high concentration of Y_{HO_2} radicals, an indicator of autoignition,[9] along the shear layers of the jet well. This is well ahead of the temperature rise from the flame. This indicates that the isothermal chemical runaway process has begun but the thermal runaway is simply waiting to happen. The high shear along the vortices' edges expose these radicals to the much hotter coflow which could initiate thermal runaway. The scatter plots from figure 6 are consistent with this explanation that leads to the lean hot mixtures igniting first. A similar mechanism was found to play a role in a turbulent autoigniting lifted slot jet simulation.[16]

III.D. Reacting round jet

The round jet is ubiquitous and a reacting round jet finds its place in a lot of applications, from Bunsen burners and blowtorches to fuel injectors in various combustion chambers. Hence the ability to perform round jet simulations is essential to address most real flames. The experiment by Cabra et. al.[5] serves as a reference for the following simulation which was carried out at a lower Reynolds number.

The jet inlet velocity is specified with the hyperbolic tangent function given by

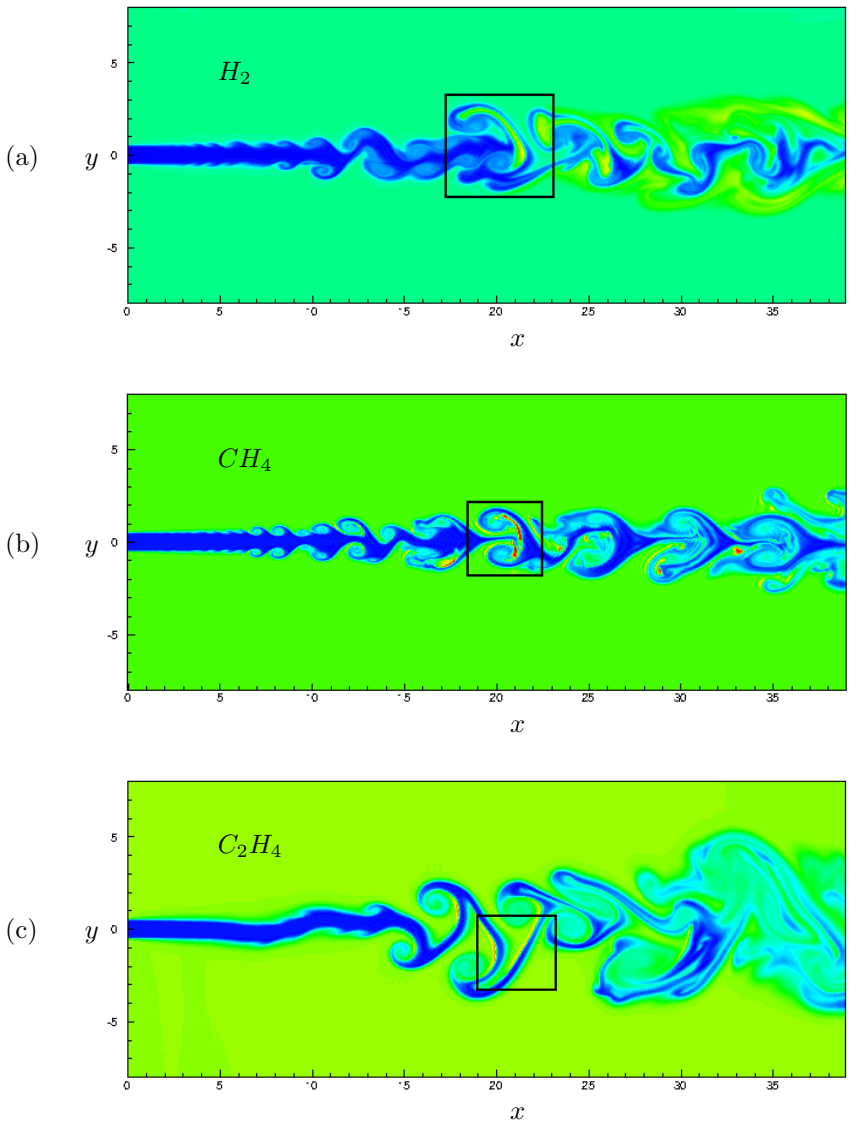

Figure 4. Normalized temperature contours for (a) H_2, (b) CH_4, and (c) C_2H_4 ranging from 1 to 8, corresponding to blue and red respectively. The box highlighting autoigniting flame kernels is shown in detail in Figure 5.

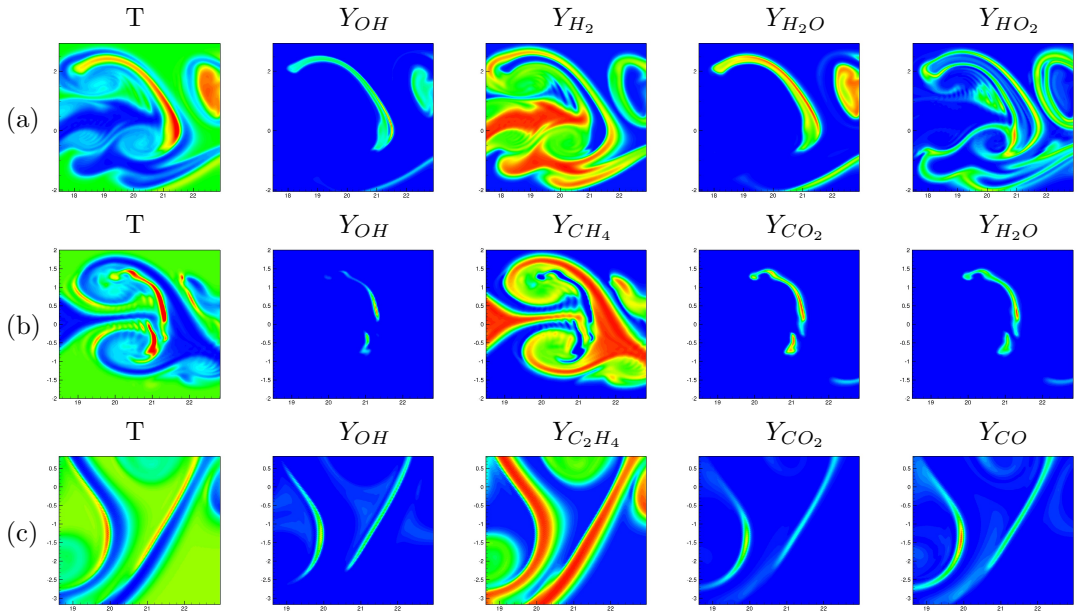

Figure 5. Autoigniting flame kernels for (a) H_2, (b) CH_4, and (c) C_2H_4.

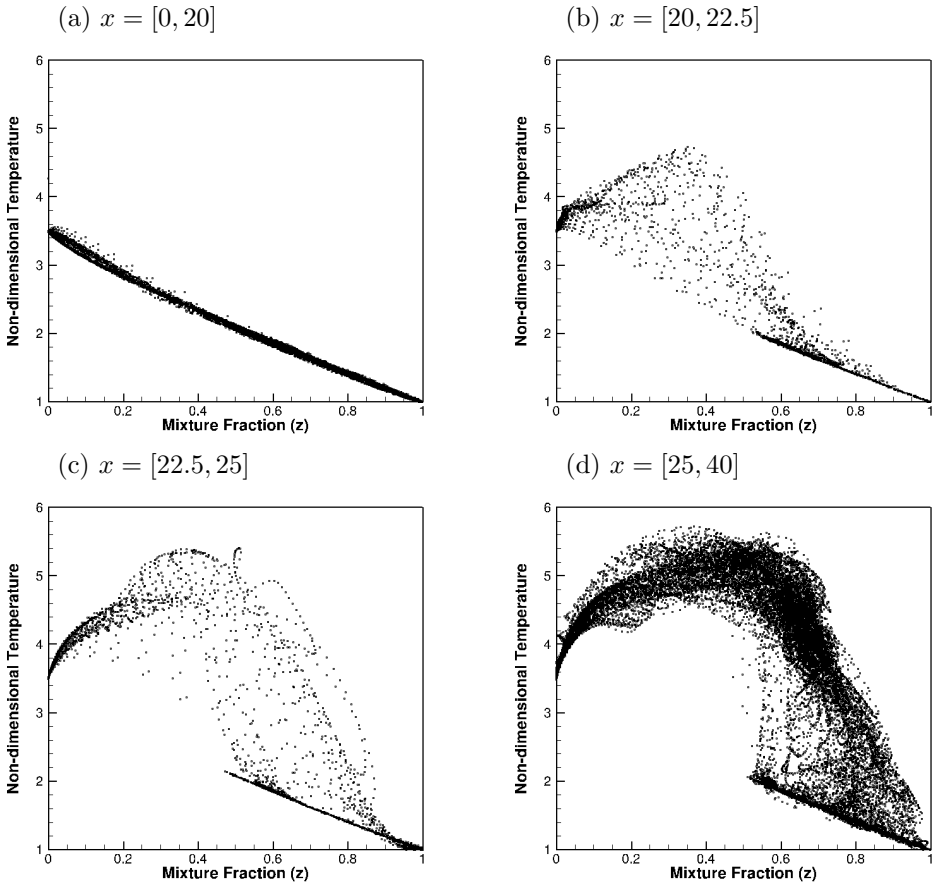

Figure 6. Scatter plot of temperature against mixture fraction at various intervals of x (in units of jet width H). The autoignition of H_2 at lean conditions is evident in (b) and (d) indicates that the lean mixtures have completely burnt, while there is still unburnt rich fuel indicated by the thick line at the bottom right corner.

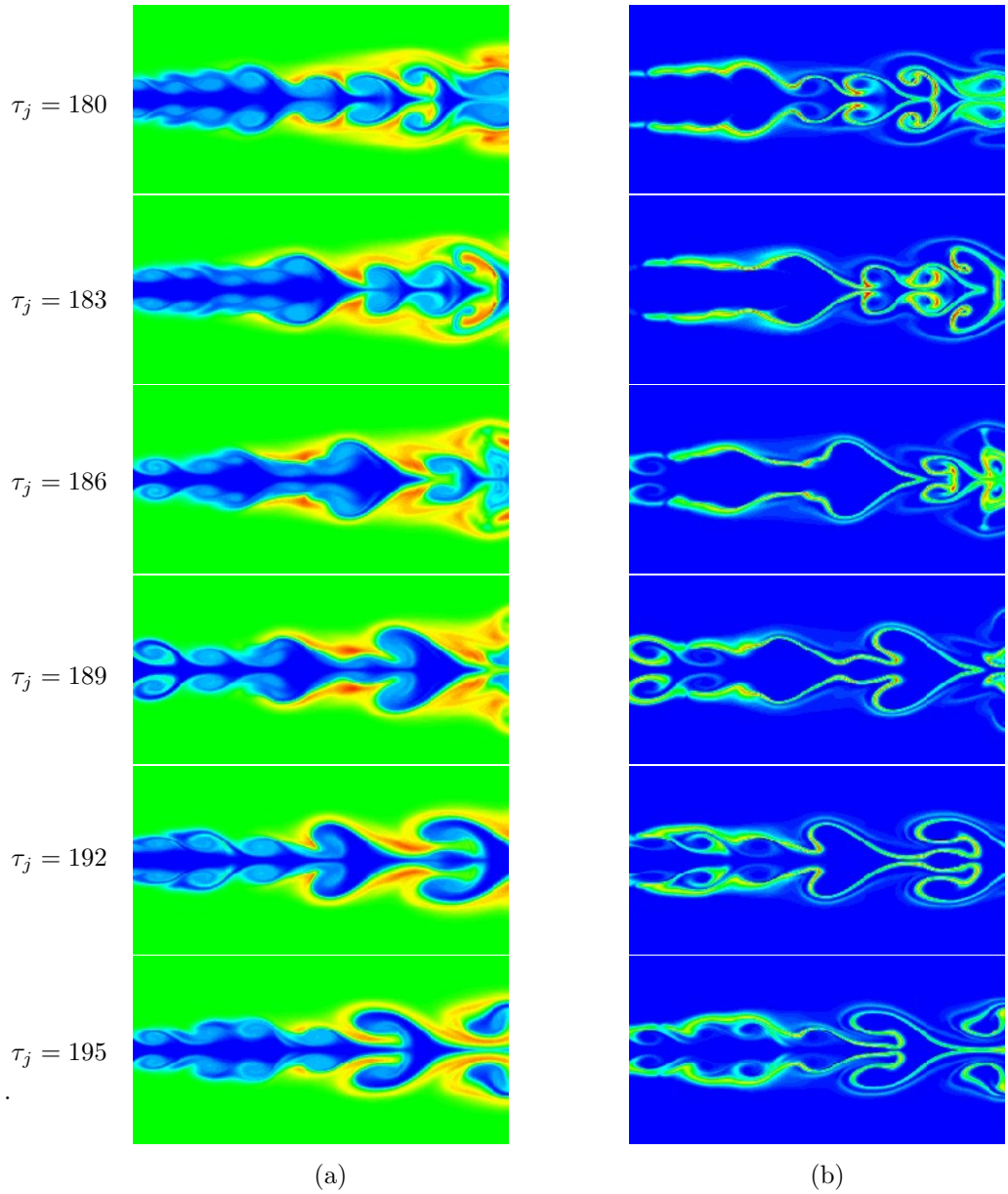

Figure 7. Temporal evolution of (a) temperature and (b) Y_{HO_2} at the base of the lifted $H_2 - Air$ flame from $\tau_j = 180$ to $\tau_j = 195$.

$$u_{in} = \frac{u_{jet} - u_{coflow}}{2}\left[1 - \tanh\left(\frac{r - D/2}{2\delta}\right)\right] + u_{coflow} \tag{27}$$

For this calculation, $\delta = 0.01D$. The Reynolds number of the jet is $Re_{jet} = 7200$ and the domain size is $40D\times\ 40D\times\ 40D$. Non-reflecting boundary conditions[14] are applied at the side and exit boundaries. Turbulent fluctuations (in the form of homogeneous isotropic turbulence) are not added to the inlet, as is commonly done in DNS studies of turbulent autoigniting flames.[16] Improved transport properties are taken into account with viscosity modified by temperature, modelled with a power law, $\mu/\mu_\circ = (T/T_\circ)^{0.67}$, and the different species are allowed to have different Schmidt numbers.[17] The effect of Lewis numbers on hydrogen flames is important and can affect autoignition times and intensities.[3,18] This simulation took a total of 0.3 million cpu-hours and was run on 1024 cpu-cores for 12.5 days for 1 flow-through time of the domain.

At these conditions, a laminar flame close to the inlet is observed. Figures 8(a) and 8(b) show the contours of temperature and Y_{OH} which are correlated with a lifted flame height of $x = 4D$. Y_{HO_2} in 8(c) however is leading the flame by almost one jet diameter, again indicating an autoignition based flame stabilization. Figure 9 illustrates an instantaneous cutaway of isosurfaces and we can see the substantial buildup of Y_{HO_2} radicals followed by the temperature increase.

A plausible reason for this flame remaining laminar in spite of the high Reynolds number can be down to the high viscosity of the hot coflow. The effect of hydrogen's low Lewis number also leads to faster ignition[3] and further increases the temperature and hence viscosity downstream of the flame. This effect is also clear in figure 8(d) where the mixture fraction shows increased diffusion downstream of the flame anchor location.

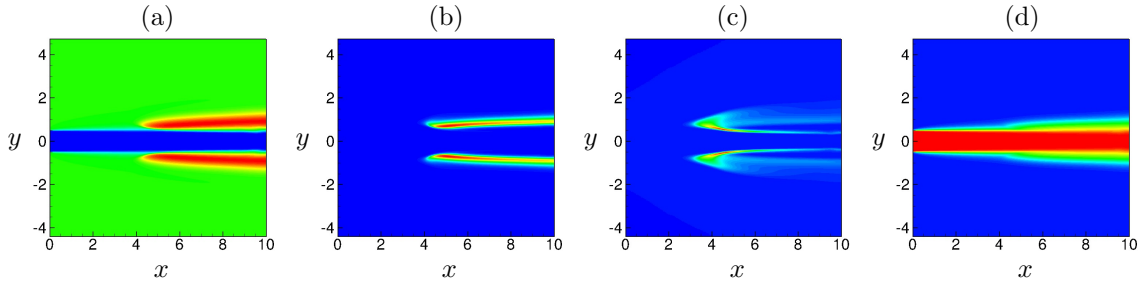

Figure 8. Contour plots of (a) Temperature, (b) Y_{OH}, (c) Y_{HO_2}, and (d) Mixture fraction ζ for the round jet.

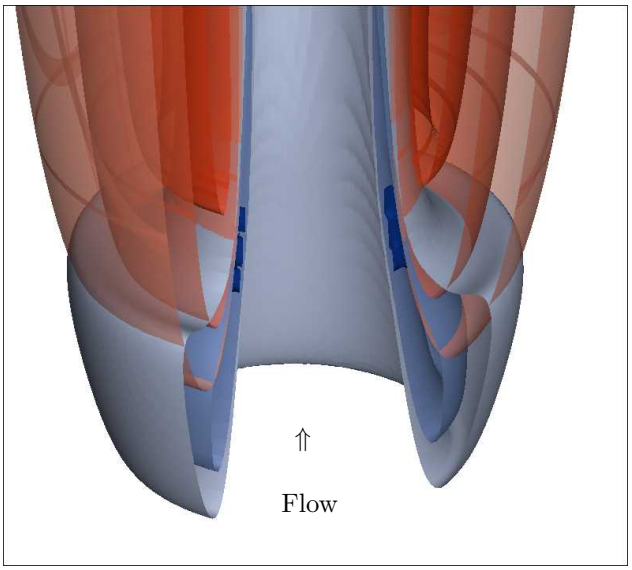

Figure 9. Flame cutaway superposing the two sets of isosurfaces, the bluish-gray isosurfaces of Y_{HO_2} positioned below the orange temperature isosurfaces indicate that the flame is stabilized by autoignition.

IV. Summary and future work

Ongoing work on the development of an algorithm to solve turbulent reacting flows is presented. The semi-implicit source term discretization mollifies the stiffness associated with the chemical source terms while simultaneously allowing explicit methods for advection and diffusion. This segregated formulation allows us to independently modify the compressible Navier-Stokes, species and chemical source term parts of the complete solver. Colocated variable storage allows this algorithm to be extended to structured and unstructured formulations seamlessly. The chemical mechanism module allows us to simulate multiple fuels easily and the simulations in this paper demonstrate this capability.

Future work includes the simulation of the experimentally observed autoigniting flames at identical laboratory conditions. The unstructured solver[4] has been used for preliminary non-reacting simulations of a scramjet inlet geometry (figure 10, based on the experiments by Gamba et al[19]). High fidelity simulations of (detailed-chemistry) reacting turbulent flow in this geometry will provide very useful understanding of issues pertinent to scramjet engines.

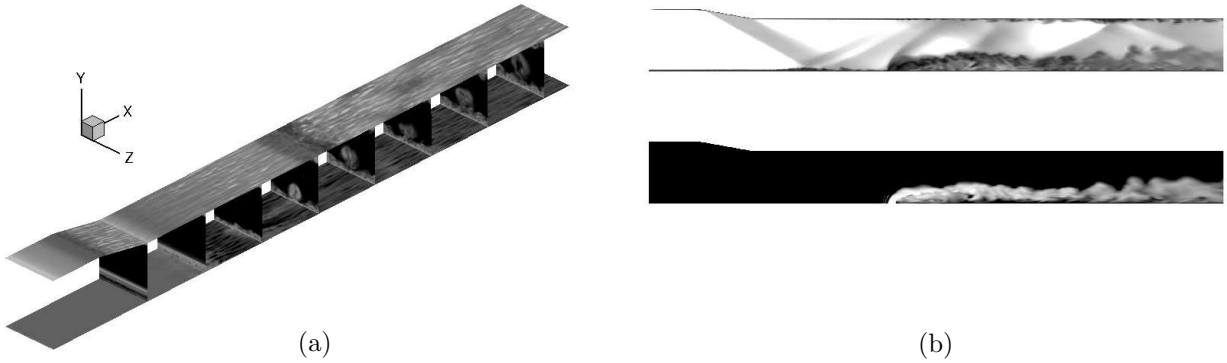

Figure 10. (a) Isometric visualization of non-reacting flow in a scramjet inlet geometry at $M_\infty = 2.9$. Figure shows the computational domain, and contours of ω_z on the top and bottom walls, contours of vorticity magnitude on the end planes. (b) Contours of (top) temperature, and (bottom) passive scalar concentration on the symmetry plane. Note that the flow features include a jet in crossflow, shock-boundary layer interaction, and a transition to turbulence.

Acknowledgements

Computer time for the simulations was provided by the Minnesota Supercomputing Institute (MSI).

References

[1]Vervisch 1, L., Hauguel, R., Domingo, P., and Rullaud 2, M., "Three facets of turbulent combustion modelling: DNS of premixed V-flame, LES of lifted nonpremixed flame and RANS of jet-flame," *Journal of Turbulence*, 2004, pp. N4.

[2]Doom, J., Hou, Y., and Mahesh, K., "A numerical method for DNS/LES of turbulent reacting flows," *Journal of Computational Physics*, Vol. 226, No. 1, 2007, pp. 1136 – 1151.

[3]Doom, J. and Mahesh, K., "Direct numerical simulation of auto-ignition of a hydrogen vortex ring reacting with hot air," *Combustion and Flame*, Vol. 156, No. 4, 2009, pp. 813 – 825.

[4]Park, N. and Mahesh, K., "Numerical and modeling issues in LES of compressible turbulent flows on unstructured grids," *AIAA Paper 2007–722*, 2007.

[5]Cabra, R., Myhrvold, T., Chen, J. Y., Dibble, R. W., Karpetis, A. N., and Barlow, R. S., "Simultaneous laser raman-rayleigh-lif measurements and numerical modeling results of a lifted turbulent H2/N2 jet flame in a vitiated coflow," *Proceedings of the Combustion Institute*, Vol. 29, 2002, pp. 1881–1888.

[6]Dally, B. B., Karpetis, A. N., and Barlow, R. S., "Structure of Turbulent Nonpremixed Jet Flames in Hot Dilute Coflow," *Proceedings of the Combustion Institute*, Vol. 29, 2002, pp. 1147–1154.

[7]Mastorakos, E., Markides, C., and Wright, Y. M., "Hydrogen autoignition in a turbulent duct flow: Experiments and Modelling," *Conference on Modelling Fluid Flow*, 2003.

[8]Oldenhof, E., Tummers, M., van Veen, E., and Roekaerts, D., "Ignition kernel formation and lift-off behaviour of jet-in-hot-coflow flames," *Combustion and Flame*, Vol. 157, No. 6, 2010, pp. 1167 – 1178.

[9]Mastorakos, E., "Ignition of turbulent non-premixed flames," *Progress in Energy and Combustion Science*, Vol. 35, No. 1, 2009, pp. 57 – 97.

[10]Mueller, M. A., Kim, T., Yetter, R. A., and Dryer, F. L., "Flow Reactor Studies and Kinetic Modeling of the H2/O2 Reaction," *International Journal of Chemical Kinetics*, Vol. 31, 1999, pp. 113–125.

[11]Smith, G. P., Golden, D. M., Frenklach, M., Moriarty, N. W., Eiteneer, B., Goldenberg, M., Bowman, C. T., Hanson, R. K., Song, S., Gardiner, W. C., Jr., V. V. L., and Qin, Z., *http://www.me.berkeley.edu/gri_mech/*.

[12]Sankaran, R., Hawkes, E., Chen, J., Lu, T., and Law, C., "Structure of a spatially developing turbulent lean methane air Bunsen flame," *Proceedings of the Combustion Institute*, 2007, pp. 1291–1298.

[13]Wang, H., Personal communication, 2012.

[14]Poinsot, T. J. and Lele, S. K., "Boundary conditions for direct simulations of compressible viscous flows," *Journal of Computational Physics*, Vol. 101, 1992, pp. 104–129.

[15]Mastorakos, E., Baritaud, T., and Poinsot, T., "Numerical simulations of autoignition in turbulent mixing flows," *Combustion and Flame*, Vol. 109, No. 12, 1997, pp. 198 – 223.

[16]Yoo, C. S., Sankaran, R., and Chen, J. H., "Three-dimensional direct numerical simulation of a turbulent lifted hydrogen jet flame in heated coflow: flame stabilization and structure," *Journal of Fluid Mechanics*, Vol. 640, 2009, pp. 453–481.

[17]Hawkes, E. R. and Chen, J. H., "Direct numerical simulation of hydrogen-enriched lean premixed methane-air flames," *Combustion and Flame*, Vol. 138, 2004, pp. 242–258.

[18]Doom, J. and Mahesh, K., "DNS of auto-ignition in turbulent diffusion H_2/air flames," 2009.

[19]Gamba, M., Miller, V. A., Mungal, G., and Hanson, R. K., "Ignition and Flame Structure in a Compact Inlet/Scramjet Combustor Model," *AIAA Paper 2011–2366*, 2011.